Research on Corrections of CFD Simulation Calculation Method for Complex Shaped Cavity Flow Based on the Wind Tunnel Test Data

Abstract: A modified CFD calculation method of Detached Eddy Simulation (DES) on flow field and noise distributions of a 3-dimensional complex shaped cavity is proposed in this paper. It has been proved through analysis as well as wind tunnel test that the modified DES method could capture the flow phenomenon in the cavity. Under transonic or supersonic flow conditions, the DES method could greatly improve the calculation accuracy by using LES's fine simulation function in the detached areas in the rear part of the cavity. Wind tunnel test data shows the OASPLs' error of the proposed method is less than 2%, and the pressure fluctuation spectrums is also in compliance with the test data.

Key words: cavity flow; Detached Eddy Simulation (DES); overall sound pressure level (OASPL); wind tunnel test

0 Introduction

Recently cavity flow has received considerable attention in the field of flow mechanism research as well as engineering application. In many cases, such as aircraft flying with an opened equipment cabin, automotive driving with an opened sunroof etc., there exist typical cavity flow phenomenon. The cavity flow field has strong vibration characteristic induced by severe boundary layer separation. Moreover, the unsteady flow fluctuation generated by this characteristic is a main source of generating noises in aircrafts, automotives and other products, as well as bad vibration around the nearby cavity structure, which is critical to the performance of the product. Therefore, cavity flow has

become an increasing hot research area.

To solve the cavity flow problem, J.E.Rossiter (1964)[5] had conducted an experimental study by using high frequency pressure sensors and flow visualization technology. He put forward a physical model based on vortex shedding and sound propagation phenomena, and deduced the relationship formula between dominant frequency of fluctuation and flow velocity/cavity length depth ratio along with other parameters:

$$f = \frac{U}{L}\frac{(m-r)}{\left(M/a_e/a_c+1/K\right)}$$

This formula is often referred as the basic method for predication of cavity flow mechanism and vibration. Smith and Shaw (1975)[1] had analyzed a lot of flight data and wind tunnel test data, and proposed an engineering method for predicting the sound pressure level in the cavity. This method has a wide application range and high engineering values. R. E. Dix and R. C. Bauer (2000)[2] had computed out the pressure fluctuation spectrums by adopting Chapman-Korst' s turbulence mixing theory and cavity tone as response functions, which are comparable to the experimental data. However, these empirical formulas are all confined to the regular two-dimensional rectangular cavity, and so far studies on the complex shape cavity flow are rarely seen. (l

On the other hand, modern computational methods and capabilities provide new chance of CFD numerical simulation for cavity flow. S. J. Lawson (2010)[7] built a geometry model of aircraft equipment cabin appearance, and predicted the cavity flow field by using CFD numerical

method based on DES hybrid model, but this simulation hadn't been verified by the experiment result. R. H. Nichols and Shawn Westmoreland (2007)[4] compared the numerical simulation results for standard separation model (WICS, L/D=4.5 and L/D=9) and the B-1B aircraft's opened front weapon bay respectively by using Euler Equations, Navier-Stokes Equations with no turbulence model, unsteady Reynolds Averaged Navier-Stokes (RANS) Equations with transport turbulence model and the Detached Eddy Simulation Model (DES) which combines features of classical RANS formulations with elements of Large Eddy Simulations (LES) methods. They found out that DES hybrid model has the advantage of high precision and less computation, but this research object is still simple shape cavity flow.

This paper focuses on the 3D complex shaped cavity flow and carries out CFD simulation analysis of complex cavity under subsonic, transonic and supersonic conditions. Wind tunnel test data with the same geometry and flow conditions is used for validation.

1 Grid Model Composition

Figure 1. shows the geometrical appearances of CFD simulation and wind tunnel test in this paper, with the following properties: a) The bottom surface of the cavity is gradually deeper along the flow direction. b) transition at the middle along the span-wise is not smooth and c) the angle between the side surface and the bottom surface is not a right angle, and there is a middle panel that separates the left and the right half cavity. With these properties

present, even if the appearance of the rectangular cavity is simple, complex change of the deep section in the cavity lead to obvious differences between the 3-dimensional and 2-dimensional displays in terms of cavity flow phenomenon.

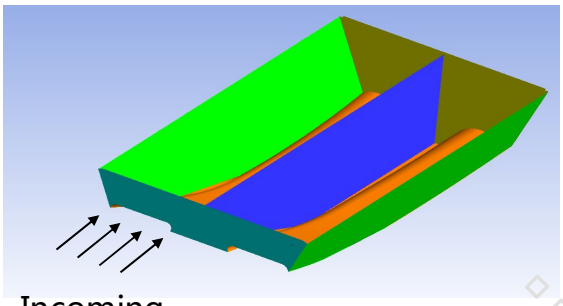

Figure 1 the complex cavity geometry

Un-structured grid system (mainly tetrahedral mesh, as shown in figure 2) is used to distribute space for the 3D complex shaped cavity flow field. The maximum grid size is 0.5mm. 20 grid knots have been assigned within the range of 2 mm near each wall cavity surface with 1.2 index growth rate. A triangular prism shaped boundary layer is formed by these 20 grid knots to capture the flow velocity change in the principle of logarithm and the development and separation pattern of the boundary layer near the cavity surface.

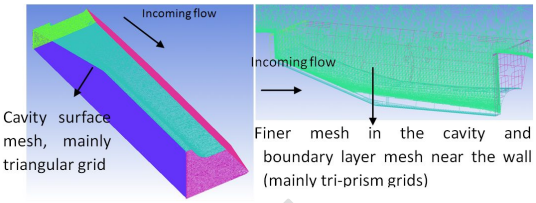

Figure 2 the complex cavity flow field grid system

The total number of half model grids is at 15.6 million, while for boundary layer grids at 11.65 million and nodes at 6.57 million respectively. There is no negative volume grid or excessive distortion grid, mesh density in the cavity is high enough, and this grid system is obtained through analysis of simulation optimization based on the wind tunnel test data where the simulation results have shown that this grid system is suitable for capturing the cavity flow fluctuation mechanism developed from boundary layer separation.

2 Numerical Methodology

DES hybrid model which combines features of classical RANS formulations with elements of LES methods is used in the CFD simulation of complex cavity flow in this paper, i.e., RANS is used inside attached and mildly separated boundary layers. Additionally, LES is applied in massively separated regions.

In massively separated regions (using LES method) the governing equations for LES are obtained from filtering the time-dependent Navier-Stokes equations in the physical space. The filtering process effectively filters out eddies whose scales are smaller than the filter width or grid spacing used in the computations. The large scale turbulent flow is solved directly and the influence of the small scales is taken into account by appropriate sub grid-scale (SGS) models. The sub grid-scale stress is defined as $\tau_{ij}=\overline{U_iU_j}-\bar{U}_i\bar{U}_j$, then the filtered N-S equation can be written in the following way:

$$\frac{\partial(\rho\bar{U}_i)}{\partial t}+\frac{\partial(\rho\bar{U}_i\bar{U}_j)}{\partial x_j}=-\frac{\partial\bar{p}}{\partial x_i}+\mu\frac{\partial^2\bar{U}_i}{\partial x_j\partial x_i}-\frac{\partial(\rho\tau_{ij})}{\partial x_j} \qquad (1)$$

The hypothesis that Reynolds stress tensor is proportional to rate of strain tensor could be used to close the equation group:

$$\tau_{ij}-\frac{1}{3}\tau_{kk}=-\left[C_S(vol)^{1/3}\right]^2\cdot|\bar{S}|\cdot\left(\frac{\partial\bar{U}_i}{\partial x_j}+\frac{\partial\bar{U}_j}{\partial x_i}\right) \qquad (2)$$

The value of Smagorinsky contant C_S depends on the research flow questions and grid distribution, generally is between 0.065 and 0.25. It this work 0.1 was used through computation and comparison.

Inside attached and mildly separated boundary layers, RANS equations and SST turbulence model were used. Flow parameters are divided into average and fluctuating quantities, where the momentum equation and

the energy equation generate respectively Reynolds stress items $\rho\overline{uu}$ and Reynolds flux items $\rho\overline{uh}$:

$$\frac{\partial(\rho\bar{\mathbf{U}})}{\partial t}+\nabla\bullet\left(\rho\bar{\mathbf{U}}\bar{\mathbf{U}}\right)=\nabla\bullet\left(\boldsymbol{\tau}-\rho\overline{\mathbf{uu}}\right)+\bar{\mathbf{S}}_M \qquad (3)$$

$$\frac{\partial(\rho\bar{h}_{tot})}{\partial t}-\frac{\partial\bar{p}}{\partial t}+\nabla\bullet\left(\rho\bar{\mathbf{U}}\bar{h}_{tot}\right)=\nabla\bullet\left(\lambda\nabla\bar{T}-\rho\overline{\mathbf{u}h}\right)+\nabla\bullet\left(\bar{\mathbf{U}}\bullet\bar{\boldsymbol{\tau}}\right)+\bar{\mathbf{S}}_E \qquad (4)$$

SST（The Shear Stress Transport）model then uses turbulence kinetic energy k and turbulent frequency ω equations to solve the transport of Reynolds shear stress and close the equation group:

$$\frac{\partial(\rho k)}{\partial t}+\nabla\bullet(\rho\mathbf{U}k)=\nabla\bullet\left[\left(\mu+\frac{\mu_t}{\sigma_{k3}}\right)\nabla k\right]+p_k-\beta'\rho k\omega \qquad (5)$$

$$\frac{\partial(\rho\omega)}{\partial t}+\nabla\bullet(\rho\mathbf{U}\omega)=\nabla\bullet\left[\left(\mu+\frac{\mu_t}{\sigma_{\omega 3}}\right)\nabla\omega\right]+(1-F_1)2\rho\frac{1}{\sigma_{\omega 2}\omega}\nabla k\nabla\omega+\alpha_3\frac{\omega}{k}p_k-\beta_3\rho\omega^2 \qquad (6)$$

In the area of automatic partitioning strategy, this paper chooses DES method proposed by Strelets. SST-RANS model or LES model is chosen based on the turbulent length L_t which is predicted by the RANS model. If L_t is larger than the local grid spacing, computation will automatically switch from the SST-RANS model to an LES model, at the same time the local grid spacing Δ will be used in the computation of the dissipation rate in the equation for the turbulent kinetic energy.

This paper numerically discretizes the government equations based on finite volume method (FVM). The unsteady terms in the equations are discretized by a second order backward Euler different schemes, and the dissipation and pressure gradient terms uses shape functions in the finite element method in the process of numerical discretization, because of the need to use element integration point values of the flow parameters and their derivatives.

Near the cavity walls, this paper uses wall function method. The values

of turbulence frequency ω near walls are given by the logarithmic relation of flow parameters near walls, and government equations near walls are then modified to ensure the accuracy and stability of the simulations.

Using grid system generated in section 1 and numerical methodology set up in this section, considering moderate (5%) turbulence intensity in the incoming flow, and using heat insulation and non slip boundary condition on the cavity wall surfaces, this paper runs CFD iterative calculation program to solve the unsteady flow field. First, a steady flow field distribution is obtained for every incoming flow condition, which is then used as initial conditions for the corresponding unsteady simulation. In the simulation time-step is set to 0.1 ms, while the total simulation time is 1 s in order to obtain the flow parameter of 10 kHz frequency resolution.

Table 1 CFD numerical methodology informations

Numerical Methodology		Grid and Simulation Informations	
criticization of Dissipation Terms	High Resolution Scheme(2 order)	Total Number of Grids	31.2 millions
Discretization of Unsteady Terms	Backward Euler Scheme(2 order)	First Layer BL Mesh Height	0.01 mm
Turblence Model	RANS/LES(DES）	BL Mesh Layers	20
near-wall treatment	Wall function	Total Height of BL Mesh	2 mm
Time-step	0.0001s	Computation Time	One week
Total Time	1s	Computation condition	32 cpus

3 Result and Discussion

Through CFD computation the complex cavity flow field evolutions in different incoming flow conditions have been obtained, and residuals of all the results have met the requirement

(the rms value<1e-4). This section will emphatically introduce and discuss the characters of the cavity flow field evolution and flow parameter fluctuation. Firstly, typical case result will be chosen to analyze the complex cavity flow structures and phenomena. Secondly, pressure signals at the same places as measured in the wind tunnel test will be processed to compare with test data, analyze the variation law of flow field distribution, and validate the numerical method.

3.1 Typical Flow Field Distribution and Evolution

Computation results and analysis of complex cavity flow phenomena for a typical case where Ma=0.85 is discussed in the following..

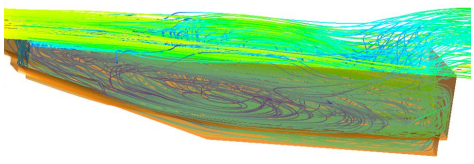

Figure 3 typical streamline distribution in the complex cavity flow at some instant

Figure 3 shows the cavity surface (transparent display) and streamline distribution. The disorder degree of the complex cavity flow can be clearly seen, and the vertex that filled in the cavity has also confirmed Rossiter test observation about large scale structures formed in the cavity. The regional fluid pulsation was aggravated by flow reverse of large amounts of fluid at the back of the cavity and the periodical mass exchange with exterior space. Therefore, back part is the worst area of noise environment in the cavity flow field.

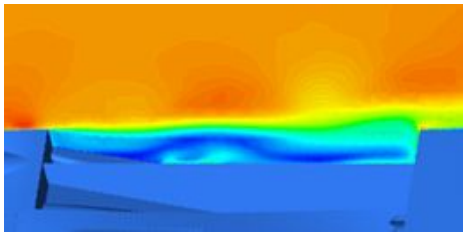

Figure 4 typical Mach number distribution in the complex cavity flow at some instant

The visual image of the shear layer

can be clearly seen in Figure 4. The boundary layer, originally thin and adhesive on the front wall, separates into a shear layer at the down step surface. Because of the overall shear layer flap up and down movement, the flow field in this area has the strongest non-steadiness. On the other hand, smoothness of the calculation results has verified that the computational grid density could meet the calculation requirement in this flow field. Besides, fluid in the cavity stays in the approximate stationary state when the cabin was closed, so the velocity here is still comparably small after it' s opened. The biggest characteristic of open cavity is that the shear layer will travel from two spatially separated parts, and these differences on the flow speed and density will cause periodical mass exchange at the back part. Therefore, the complex cavity flow discussed in this paper still presents the characteristics of the open cavity flow in the high speed incoming flow conditions, and this conclusion has also been confirmed by the wind tunnel test.

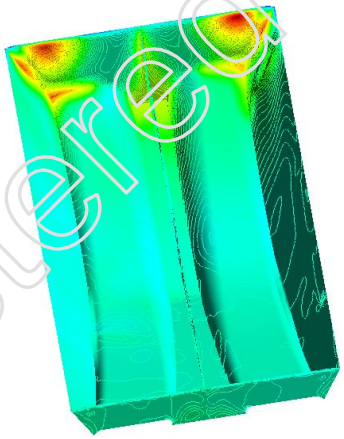

Figure 5 typical pressure distribution in the complex cavity flow at some instant

Figure 5 shows the great difference between pressure distribution on the back wall and on other walls in the cavity. A few concentrated high pressure areas just shows the trailing edge points on which shear layer fluid directly impact, and this points can also move on the back wall as the change of time. The strength difference of the

fluid impacting makes the rear wall pressure fluctuate, and back wall uneven pressure distribution is caused by the 3D effect of the complex cavity.

3.2 fluctuating pressure OASPL data processing and analysis

This paper also processed data recorded from pulse pressure sensors (their position are as shown in Figure 6) placed in wind tunnel test, as well as pressure evolution data of the corresponding points extracted from the unsteady flow field results, and compared the OASPL parameters which reflect the overall fluctuating level. Through data analysis effect on the accuracy improvement of DES model compared with RANS+SST model is obvious.

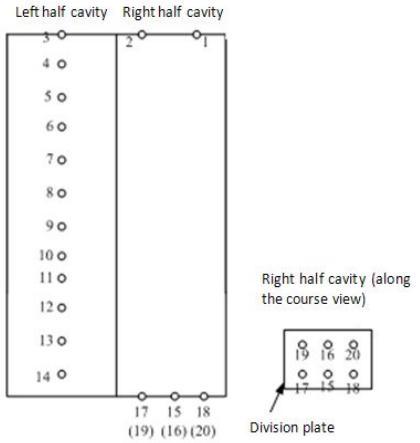

Figure 6 pulse pressure sensor positions in the wind tunnel test

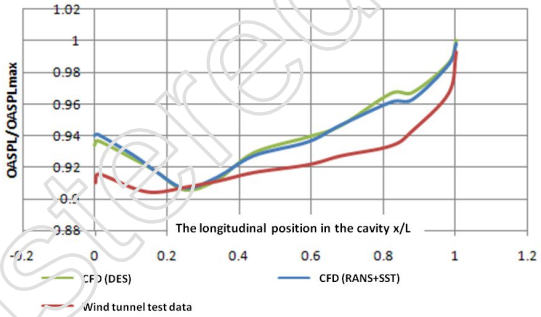

Figure 7 Ma=0.85 OASPL distribution in the cavity

From Figure 7, it can be easily found that the calculation result of CFD is slightly larger than the wind tunnel test result, but the distribution regulars are similar. This confirms the analysis on the flow structure around the cavity. The large scale structure mainly distributes in the back area of x/L>0.3 and the deviation from test data of OASPL may be introduced by

the incoming turbulence intensity difference between simulation and wind tunnel. Additionally, as subsonic flow disturbances can be transferred to the whole flow field, the DES model with Strelets correlation used in this paper doesn’ t have higher precision compared with traditional RANS+SST model. However, error within 5% is acceptable in engineering.

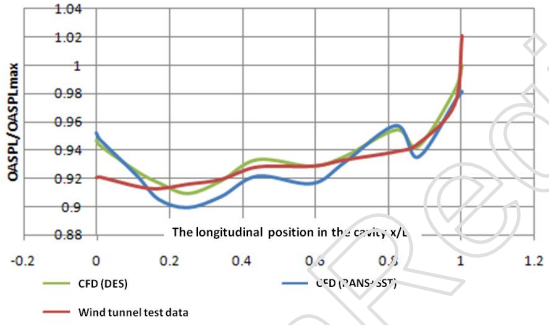

Figure 8 Ma=1.05 OASPL distribution in the cavity

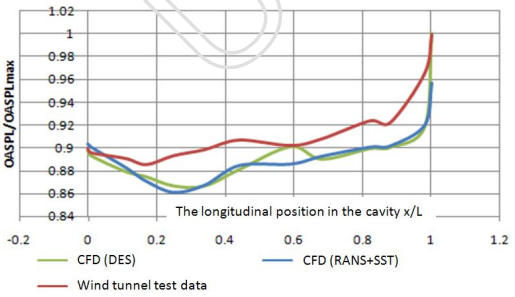

Figure 9 Ma=1.5 OASPL distribution in the cavity

In the conditions of transonic and supersonic the accuracy of DES model improves significantly (as shown in Figure 9). The OASPL distribution trend along the longitudinal direction obtained from DES simulation is consistent with the test result, and computational errors of most points are less than 2%. Therefore, the grid system and DES model used in this paper are suitable for the complex cavity flow simulations, and has the ability to distinguish the lager-scale vortex structure movement and pressure fluctuations where RANS+SST model doesn’ t.

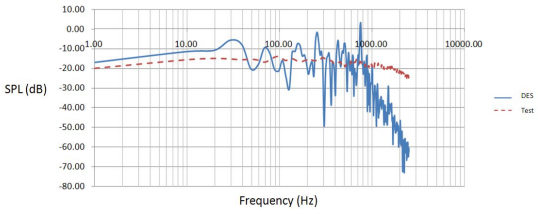

Figure 10 Ma=1.05 SPL spectrum of pressure point 14 on the rear wall of the cavity

Figure 10 shows the cavity rear typical acoustic pressure spectrum distribution. It can be found that, in the rear part where the large scale vortex is

the dominant structure in the flow field, pressure spectrums obtained using DES model simulation are very close to the test result, because LES is directly applied in these massively separated regions in the DES model. Besides, as the effective sampling frequency is only 5K, while the sampling frequency of pulse pressure sensors in the test reaches 40K, therefore simulation and test result didn' t converge on the spectrum beyond 1000 Hz .

4 Conclusion

This paper used the DES model to construct CFD simulation method on the base of the wind tunnel test data, and carried out CFD simulation for a complex shape cavity flow. This method has been found having higher precision than traditional RANS+SST model.

Conclusions obtained through calculation are as following:

(1) DES model can realistically describe flow phenomena around the cavity. Similar phenomena have been found in the computation and wind tunnel test result which verifies the DES model simulation.

(2) Through monitoring typical point pressure signals' OASPLs at front, middle and rear part of the cavity, it has been found that computation result errors of DES model for most of points in subsonic conditions are less than 5% compared with wind tunnel test. And in the conditions of transonic and

supersonic, the advantage of DES model is more obvious, because using LES model in the massively separated regions is more suitable for the complex cavity flow. So it has improved computational precision greatly (error within 2%).

(3) Through spectral analysis, we can find that flow around the front part of cavity is controlled by boundary layer separation process where results of DES and SST model have little difference, but in the middle and rear part, because of massive separation the simulation effect of DES model is obviously better.

Reference Documentations:

[1] D.L. Smith & L.L. Shaw. Prediction of the pressure oscillations in cavities exposed to aerodynamic flow. AFFDL-TR-75-34, 1975.

[2] R. E. Dix, and R. C. Bauer. Experimental and Predicted Acoustic Amplitudes in a Rectangular Cavity. AIAA paper 2000-0472, 2000.

[3] Shia-Hui Peng. Unsteady RANS Simulation of Turbulent Flow Over a Weapon-Bay Cavity [R]. FOI-R-1983-SE, 2006.

[4] R. H. Nichols and Shawn Westmoreland. Comparison of CFD Approaches for Simulating Flow inside a Weapons Bay. AIAA Paper 2006-0455.

[5] J. E. Rossiter. Wind-tunnel experiments on the flow over rectangular cavities at subsonic and transonic speeds. Aeronautical research council reports and memoranda no.3438, 1964.

[6] Ning Zhuang. Experimental investigation of supersonic cavity flows and their control. PhD thesis, College of engineering, the Florida State University, 2007.

[7] S.J. Lawson and G.N. Barakos. Evaluation of DES for Weapons Bays in UCAVs. AIAA paper 2010-1425.

Author Brief Introduction:

Huang Hu, Tel: 028-65020253, Email: yellowtiger19860603@126.com.cn

Jin Wei, Tel: 028-85508646
Fu Huanbing, Tel: 028-85509930

Address: No. 1610, Riyue Avenue, Qingyang District, Chengdu
Postal code: 610091